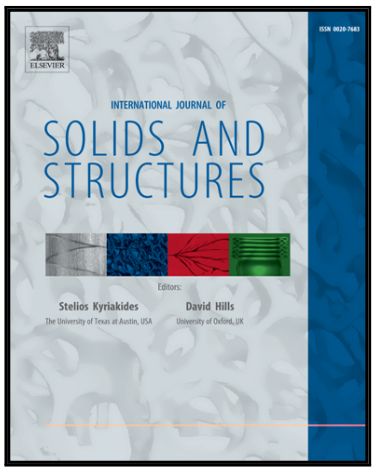

Distance of a stiffness tetrad to the symmetry classes of linear elasticity

Martin Weber, Rainer Glüge, Albrecht Bertram

PII: S0020-7683(18)30339-1
DOI: https://doi.org/10.1016/j.ijsolstr.2018.08.021
Reference: SAS 10095

To appear in: *International Journal of Solids and Structures*

Received date: 8 May 2017
Revised date: 7 August 2018
Accepted date: 22 August 2018

Please cite this article as: Martin Weber, Rainer Glüge, Albrecht Bertram, Distance of a stiffness tetrad to the symmetry classes of linear elasticity, *International Journal of Solids and Structures* (2018), doi: https://doi.org/10.1016/j.ijsolstr.2018.08.021

Distance of a stiffness tetrad to the symmetry classes of linear elasticity

Martin Weber[1], Rainer Glüge[1], Albrecht Bertram[2]
[1]Institute of Mechanics, Otto von Guericke University Magdeburg, 39106 Magdeburg, Germany
[2]Institute of Mechanics, Technical University of Berlin, 10623 Berlin, Germany

August 28, 2018

In the scope of linear anisotropic elasticity, the fourth-order elasticity tensor or tetrad has to be identified. This can be done either by measurements or by numerical simulations. An important task is then to identify a given tetrad, probably with some experimental or numerical scattering, with one of the symmetry classes. For this purpose one needs a distance function between a given tetrad and the class of all tetrads with a particular symmetry, which is zero if the tetrad obeys this symmetry, or non-zero otherwise. In this paper we present a fast method to solve these problems. We firstly introduce the 8^{th} order projectors that map any stiffness tetrad into the part that is invariant under the action of a specific fixed symmetry group. For this purpose we consider the seven out of the eight symmetry classes that are distinguishable in linear elasticity. Secondly, since the symmetry axes of the specific stiffness tensor under consideration is generally not aligned with the used tensorial basis of the projector, we need to rotate the sample stiffness. The optimal orientation is obtained when the distance between the rotated stiffness and the rotated and projected stiffness is minimal. Thus, we need

to apply only linear mappings and minimize over three Euler angles. The latter is quite simple, as the domain of the Euler angles is periodic, and the number of local minima is limited. This procedure has the advantage that it is applicable in an algorithmic manner, and does not require an a priori identification of symmetry planes, symmetry axes or component symmetries, which are only apparent under special choices for the tensorial basis.

Keywords: stiffness tetrad; elastic symmetry; anisotropic distance function; symmetry groups

1 Introduction

Most materials, like crystals, exhibit spatial symmetries in their structure. These symmetries must be reflected in their material properties (Curie, 1894; Neumann, 1885). In particular, these symmetries must be obeyed by all material tensors which appear in the constitutive equations. Depending on the tensorial order, the symmetry requirement affects the material property tensor differently. The odd order tensors vanish in case that the material structure has centro-symmetry, i.e. that $-\boldsymbol{I}$ is in the materials symmetry group. The subgroups of the orthogonal group are for example detailed in Olive and Auffray (2014) Sec. 2.3 or Butler (1981) Sec. 5. In general, the higher the tensorial order, the more symmetries can be distinguished in the material properties. For instance, the second order heat conduction tensor is isotropic even for cubic crystals, while the fourth order stiffness tensor (tetrad) with cubic symmetry has three independent parameters, but an isotropic stiffness tetrad has only 2 independent parameters. Forte and Vianello (1996) show that in linear elasticity 8 material symmetries can be distinguished, namely triclinic, monoclinic, orthotropic, tetragonal, trigonal, hexagonal, cubic and isotropic. For a given stiffness tetrad of unknown symmetry resulting from measurement or numerical simulations the question arises to which symmetry class it belongs. Since the coefficients of the stiffness tetrad are in general not exact, the affiliation to one of the eight material symmetry classes may neither be exact. It is therefore reasonable to define a distance as a deviation measure between a stiffness tetrad and the set of all stiffness tetrads with a certain symmetry, which we will call the symmetry class. This may serve to filter stochastic scatterings from measurements, see also Guilleminot and Soize (2010); Norris (2006). Further, one may be able to reduce the complexity of the elastic model by replacing a complex (possibly triclinic) stiffness tetrad by a more symmetric candidate that is close enough to the original stiffness.

In the literature one can find several approaches to this topic. In Moakher and Norris (2006) three different distance functions are defined to determine the closest elastic tensor of arbitrary symmetry to an elasticity tensor of lower symmetry. They consider the Euclidean/Frobenius norm, the log-Euclidean norm and the Riemannian norm. In Guilleminot and Soize (2010), these distance measures are used as a starting point to determine the distances of stochastically generated stiffness tetrads to the set of transversal isotropic stiffnesses. Böhlke (2001); Fedorov (1968) use the Frobenius norm to measure the distance between two stiffness tensors as we will do later on. It has been shown by Gazis, Tadjbakhsh, and Toupin (1963) that the average group action gives a projection of a stiffness tetrad onto the subset of all stiffness tetrads with a given symmetry. In Glüge, Weber, and Bertram (2012), in the course of determining the anisotropy induced by a representative volume element (RVE) of cubic shape, a similar projection method is used to quantify the anisotropy of a stiffness tetrad and also the distance to the cubic symmetry class. In the same article one projection is onto the isotropic stiffnesses and the other one to the cubic stiffnesses of the anisotropy axes that are aligned with the RVE. Thus we do not need to find the orientation in this special situation. In the same article, a logarithmic normalization is presented, which ensures consistency in the sense that the same distance is measured if the inverse of the stiffness tetrad, namely the compliance tetrad, is considered.

When the anisotropy axes are unknown, the sought distance is w.r.t. a symmetry class, but not w.r.t. a specific symmetry group. One of the first to take the unknown orientation into account were Francois, Geymonat, and Berthaud (1998), who inspect pole figures to determine the symmetry visually. Afterwards, similar to our projection method, a so called orbit is defined as a collection of all transformations within the chosen group. In contrast to our approach, Francois, Geymonat, and Berthaud (1998) perform the minimization of the distance over the Euler angles after the projection. Further, this problem is addressed in Diner, Kochetov, and Slawinski (2011); Kochetov and Slawinski (2009), who also use the Frobenius norm and distance functions from transversal and monoclinic symmetry, respectively. They also take into account the unknown orientation of the symmetry axes or planes, minimizing over two angles. This is possible due to a simplification that is only applicable for these two symmetry classes. We will use this simplification to remove one of the Euler angles from the minimization procedure. A different approach is chosen by Zou, Tang, and Lee (2013). They determine the exact symmetry class to which a tetrad belongs by a harmonic decomposition and a multipole representation of its deviators. Then the angular deviation of the vectors

from the multipole representation is used as a distance measure. They state that *it is impossible to find a simple function to define the distance between the elastic tensor measured experimentally and its nearest possible symmetry groups*.

Outline. In this article we present a method to determine this distance. As Zou, Tang, and Lee (2013) state, we can not give a simple, closed form solution for the problem, but a fast and reliable numerical algorithm instead. To find out the closest symmetry class of the measured stiffness tetrad we determine the Euclidean distance to all possible symmetry classes by employing a projection method. Further, we need to find the closest orientation (see Cowin and Mehrabadi (1987) and Francois, Geymonat, and Berthaud (1998)). We do this by minimizing the Euclidean distance between the rotated stiffness to the rotated and projected stiffness over the three Euler angles. Although this minimization problem exhibits some peculiarities which need to be considered, it leads to a fast and robust algorithm for finding the distance to the seven non-trivial symmetry classes of linear elasticity. In addition to these distances, the algorithm gives also the elements in the respective symmetry classes that are closest to the stiffness tetrad under consideration. Finally we apply the method to stiffnesses of unknown symmetries which emerge from RVE simulations of three different sample materials.

2 Determining the distance of a stiffness tetrad to a symmetry class

2.1 Notation

A direct notation is preferred. Vectors are denoted as bold minuscules (like $\boldsymbol{e}$), second-order tensors as bold majuscules (like $\boldsymbol{Q}$ for the rotation tensor), fourth-order tensors as blackboard bold letters (like the stiffness tetrad $\mathbb{K}$) and higher order tensors as blackboard bold letters with the order denoted above the letter (like the 8^{th} order tensor $\overset{\langle 8 \rangle}{\mathbb{P}}$). The dyadic product and scalar contractions are denoted like $(\boldsymbol{a} \otimes \boldsymbol{b} \otimes \boldsymbol{c}) \cdot\cdot (\boldsymbol{d} \otimes \boldsymbol{e}) = (\boldsymbol{b} \cdot \boldsymbol{d})\,(\boldsymbol{c} \cdot \boldsymbol{e})\,\boldsymbol{a}$, with $\cdot$ being the usual scalar product between vectors. The combination of the scalar products is such that an n-fold contraction of two tensors of order n inherits the positive definiteness of the scalar product between vectors. Furthermore we use the Rayleigh product denoted by $*$ which maps all base vectors of a tensor simultaneously without changing its components. More precisely, for the second or-

der rotation tensor $\boldsymbol{Q}$ and the fourth order stiffness tensor $\mathbb{K}$ the Rayleigh product is $\boldsymbol{Q} * \mathbb{K} = \boldsymbol{Q} * (K_{ijkl}\boldsymbol{e}_i \otimes \boldsymbol{e}_j \otimes \boldsymbol{e}_k \otimes \boldsymbol{e}_l \otimes) = K_{ijkl}\,(\boldsymbol{Q}\boldsymbol{e}_i) \otimes (\boldsymbol{Q}\boldsymbol{e}_j) \otimes (\boldsymbol{Q}\boldsymbol{e}_k) \otimes (\boldsymbol{Q}\boldsymbol{e}_l)$. This constitutes a linear mapping between tetrads and, thus, allows for a representation by an 8^{th} order tensor $\overset{\langle 8 \rangle}{\mathbb{P}}$. Caligraphic letters denote sets, like $\mathcal{O}rth^+$ for the set of proper orthogonal tensors. Rotations are represented by second order tensors $\boldsymbol{Q}$. The meaning of the subscripts depends on the parametrization of the rotations. In case of an axis-angle parametrization, the lower index indicates the axis and the upper index the angle, like $\boldsymbol{Q}_{\boldsymbol{e}_2}^{\pi/2}$ for a 90° rotation around the $\boldsymbol{e}_2$-axis. In case of a parametrization in Euler angles, the Euler angles are subscripts, like $\boldsymbol{Q}_{\alpha,\beta,\gamma}$. A single subscript index refers to the group element, like $\boldsymbol{Q}_1$ for the first group element, double index subscripts are used for the usual index notation. For rotations we have $\boldsymbol{Q}^T = \boldsymbol{Q}^{-1}$. In what follows, $\mathcal{G}$ is one of the subsets of $\mathcal{O}rth^+$ that forms a symmetry group that is distinguishable in linear elasticity, which is detailed in the next section. The set $\mathcal{K}$ denotes the vector space of all stiffness tetrads $\mathbb{K}$.

2.2 Definitions

Stiffness tetrad A stiffness tetrad $\mathbb{K}$ is a fourth order tensor that appears in the generalized Hooke's law. It is a linear mapping from a second order symmtric strain tensor $\boldsymbol{\varepsilon}$ into a second order symmetric stress tensor $\boldsymbol{\sigma}$,

$$\boldsymbol{\sigma} = \mathbb{K} : \boldsymbol{\varepsilon}. \tag{1}$$

It has the principle symmetry $\mathbb{K} : \boldsymbol{\varepsilon} = \boldsymbol{\varepsilon} : \mathbb{K}$ and inherits the index symmetries of the stress and strain tensors, which are the subsymmetries of $\mathbb{K}$.

Symmetry transformation A tetrad $\mathbb{K}$ is symmetric w.r.t. the rotation $\boldsymbol{Q}$ if

$$\mathbb{K} = \boldsymbol{Q} * \mathbb{K} \tag{2}$$

holds. Thus, the transformation $\boldsymbol{Q} * \mathbb{K}$ does not alter $\mathbb{K}$ and is called a symmetry transformation. The set of all such symmetry transformations form the symmetry group of the tetrad. Due to the even number of entries in $\mathbb{K}$ we have $\mathbb{K} = -\boldsymbol{I} * \mathbb{K}$. Thus, all elements from $\mathcal{O}rth^-$ can be generated by multiplying the elements of $\mathcal{O}rth^+$ with $-\boldsymbol{I}$. Therefore, it is sufficient to focus on $\mathcal{O}rth^+$ and its subgroups, the expansion to the whole $\mathcal{O}rth$ does not give any new insight for tensors of even order.

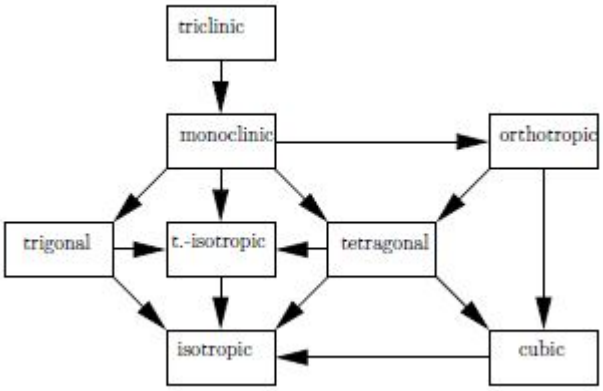

Figure 1: Symmetry inclusion scheme. The arrows indicate a subset relation, pointing from the larger set to the subset.

Symmetry group All symmetry groups $\mathcal{G} = \{\boldsymbol{I}, \boldsymbol{Q}_2, \ldots, \boldsymbol{Q}_n\}$ of solids are subgroups of the orthogonal group $\mathcal{O}rth^+$ which is closed under an associative composition $\boldsymbol{Q}_i = \boldsymbol{Q}_j \cdot \boldsymbol{Q}_k$, $\boldsymbol{Q}_{i,j,k} \in \mathcal{G}$. Further, it contains the identity $\boldsymbol{I} \cdot \boldsymbol{Q}_i = \boldsymbol{Q}_i$, by which an inverse is assigned to any group element $\boldsymbol{Q}_i \cdot \boldsymbol{Q}_i^T = \boldsymbol{I}$, which is also part of the group. All N elements $\boldsymbol{Q}_i$ can be generated from a non-unique minimum set of generators by these group operations.

One can see that an expansion of the form $\mathcal{G}^* = \{\boldsymbol{I}, \boldsymbol{Q}^T\boldsymbol{Q}_2\boldsymbol{Q}, \ldots, \boldsymbol{Q}^T\boldsymbol{Q}_N\boldsymbol{Q}\}$ with $\boldsymbol{Q} \in \mathcal{O}rth^+$ produces a symmetry group $\mathcal{G}^*$ which is isomorphic to $\mathcal{G}$. Hence, for all isomorphic groups one may choose a reference group. The eight reference groups that are used here are given in Table 1. One can sort the symmetry classes according to the set inclusion scheme given in Fig. 1, see Bóna, Bucataru, and Slawinski (2004). We refer to symmetries as higher and lower if a subset relation holds. Lower symmetries include higher symmetries as special cases, but not all symmetry classes are nested. One can see that in Fig. 1 trigonal and tetragonal symmetries are not connected by a unidirectional path of arrows, so there exists no subset relation for these two symmetries. It should be noted that one can also sort the symmetries into higher and lower by the symmetry group size N (right column in Table 1).

Symmetry class The symmetry class $\mathcal{K}_{\mathrm{sym}_i}$ denotes all stiffness tetrads for which a rotation $\boldsymbol{Q}$ can be found such that the rotated stiffness is invariant under the action of

symmetry	reference generators	indep. const. $\mathbb{K}$	no. of ele. N in $\mathcal{G}$
triclinic	$\boldsymbol{I}$ $\begin{pmatrix} 1 & 0 & 0 \\ 0 & 1 & 0 \\ 0 & 0 & 1 \end{pmatrix}$	21	1
monoclinic	$\boldsymbol{Q}^{\pi}_{\boldsymbol{e}_1}$ $\begin{pmatrix} 1 & 0 & 0 \\ 0 & -1 & 0 \\ 0 & 0 & -1 \end{pmatrix}$	13	2
orthotropic	$\boldsymbol{Q}^{\pi}_{\boldsymbol{e}_1}$, $\boldsymbol{Q}^{\pi}_{\boldsymbol{e}_2}$ $\begin{pmatrix} 1 & 0 & 0 \\ 0 & -1 & 0 \\ 0 & 0 & -1 \end{pmatrix}$, $\begin{pmatrix} -1 & 0 & 0 \\ 0 & 1 & 0 \\ 0 & 0 & -1 \end{pmatrix}$	9	4
trigonal	$\boldsymbol{Q}^{\pi}_{\boldsymbol{e}_2}$, $\boldsymbol{Q}^{2\pi/3}_{\boldsymbol{e}_3}$ $\begin{pmatrix} -1 & 0 & 0 \\ 0 & 1 & 0 \\ 0 & 0 & -1 \end{pmatrix}$, $\begin{pmatrix} -\frac{1}{2} & -\frac{\sqrt{3}}{2} & 0 \\ \frac{\sqrt{3}}{2} & -\frac{1}{2} & 0 \\ 0 & 0 & 1 \end{pmatrix}$	6	6
tetragonal	$\boldsymbol{Q}^{\pi}_{\boldsymbol{e}_1}$, $\boldsymbol{Q}^{3\pi/2}_{\boldsymbol{e}_3}$ $\begin{pmatrix} 1 & 0 & 0 \\ 0 & -1 & 0 \\ 0 & 0 & -1 \end{pmatrix}$, $\begin{pmatrix} 0 & 1 & 0 \\ -1 & 0 & 0 \\ 0 & 0 & 1 \end{pmatrix}$	6	8
hexagonal	$\boldsymbol{Q}^{\pi}_{\boldsymbol{e}_1}$, $\boldsymbol{Q}^{\pi/3}_{\boldsymbol{e}_3}$ $\begin{pmatrix} 1 & 0 & 0 \\ 0 & -1 & 0 \\ 0 & 0 & -1 \end{pmatrix}$, $\begin{pmatrix} \frac{1}{2} & -\frac{\sqrt{3}}{2} & 0 \\ \frac{\sqrt{3}}{2} & \frac{1}{2} & 0 \\ 0 & 0 & 1 \end{pmatrix}$	5	12
cubic	$\boldsymbol{Q}^{3\pi/2}_{\boldsymbol{e}_1}$, $\boldsymbol{Q}^{2\pi/3}_{\frac{1}{\sqrt{3}}(\boldsymbol{e}_1+\boldsymbol{e}_2+\boldsymbol{e}_3)}$ $\begin{pmatrix} 1 & 0 & 0 \\ 0 & 0 & 1 \\ 0 & -1 & 0 \end{pmatrix}$, $\begin{pmatrix} 0 & 0 & 1 \\ 1 & 0 & 0 \\ 0 & 1 & 0 \end{pmatrix}$	3	24
isotropic	$\boldsymbol{Q}^{\phi}_{\boldsymbol{v}}$, ϕ and $\boldsymbol{v}$ arbitrary -	2	∞

Table 1: Possible symmetries of the stiffness tetrad $\mathbb{K}$

the reference symmetry group sym_i as labeled in the first column in Table 1,

$$\boldsymbol{Q} * \mathbb{K} = \boldsymbol{Q}_j * (\boldsymbol{Q} * \mathbb{K}) \quad \forall \boldsymbol{Q}_j \in \mathcal{G}_{\mathrm{sym}_i} \quad \forall \mathbb{K} \in \mathcal{K}_{\mathrm{sym}_i} \tag{3}$$

which can be written as

$$\mathbb{O} = \boldsymbol{Q} * \mathbb{K} - (\boldsymbol{Q}_j \boldsymbol{Q}) * \mathbb{K} \quad \forall \boldsymbol{Q}_j \in \mathcal{G}_{\mathrm{sym}_i} \quad \forall \mathbb{K} \in \mathcal{K}_{\mathrm{sym}_i}. \tag{4}$$

By the properties of the Rayleigh product this may be rewritten as

$$\mathbb{O} = \mathbb{K} - (\boldsymbol{Q}^T \boldsymbol{Q}_j \boldsymbol{Q}) * \mathbb{K} \quad \forall \boldsymbol{Q}_j \in \mathcal{G}_{\mathrm{sym}_i} \quad \forall \mathbb{K} \in \mathcal{K}_{\mathrm{sym}_i} \ . \tag{5}$$

It is obvious that one can either rotate $\mathbb{K}$ and check w.r.t. the reference symmetry group or keep $\mathbb{K}$ fixed and check the rotated reference symmetry group. From a practical point of view, eq. (4) offers the advantage that the Rayleigh product with $\boldsymbol{Q}$ appears only

once in each summand, and that only one rotation (only $\boldsymbol{Q}$, not $\boldsymbol{Q}^T$) is needed.

Distance measure Let us parametrize a rotation $\boldsymbol{Q}$ by three Euler angles α, β and γ. For stiffness tetrads which do not belong to a certain symmetry class $\mathcal{G}_{\mathrm{sym}}$, a residuum remains on the left side of eq. (4), i.e.

$$\mathbb{R}_i(\alpha,\beta,\gamma) = \boldsymbol{Q}_{\alpha,\beta,\gamma} * \mathbb{K} - (\boldsymbol{Q}_i \boldsymbol{Q}_{\alpha,\beta,\gamma}) * \mathbb{K} \quad \boldsymbol{Q}_i \in \mathcal{G}_{\mathrm{sym}} \quad \mathbb{K} \in \mathcal{K}. \tag{6}$$

$\mathbb{R}_i(\alpha,\beta,\gamma)$ is a difference between stiffnesses. We obtain a relative residuum by normalizing with $\|\mathbb{K}\|$. Since $\|\boldsymbol{Q} * \mathbb{K}\| = \|\mathbb{K}\|$ we can define the relative residuum by

$$\mathbb{R}_i^*(\alpha,\beta,\gamma) = \boldsymbol{Q}_{\alpha,\beta,\gamma} * \mathbb{K}^* - (\boldsymbol{Q}_i \boldsymbol{Q}_{\alpha,\beta,\gamma}) * \mathbb{K}^* \quad \boldsymbol{Q}_i \in \mathcal{G}_{\mathrm{sym}} \tag{7}$$

with $\mathbb{K}^* = \mathbb{K}/\|\mathbb{K}\|$. We can consider the norm $\|\mathbb{R}_i^*(\alpha,\beta,\gamma)\|$ as the relative difference between some stiffness tetrad that belongs to the symmetry class $\mathcal{K}_{\mathrm{sym}}$ and the stiffness tetrad $\mathbb{K}$. The global minimum

$$d = \min_{i,\alpha,\beta,\gamma} \|\mathbb{R}_i^*(\alpha,\beta,\gamma)\| \tag{8}$$

gives the closest relative distance between $\mathbb{K}$ and all tetrads that belong to the symmetry class $\mathcal{K}_{\mathrm{sym}}$.

2.3 Minimization over the elements of the symmetry group by a projection method

The minimization over the index i that labels the group elements is carried out by a projection. This projection is basically the average under the action of all group members. It can be formulated for the seven anisotropic classes with finite group sizes N as

$$\overline{\mathbb{K}}_{\mathcal{G}} = \frac{1}{N} \sum_{z=1}^{N} (\boldsymbol{Q}_z * \mathbb{K}) \,. \tag{9}$$

Because of the linearity of the Rayleigh product in the second argument

$$\boldsymbol{Q} * (\alpha \mathbb{K}_1 + \mathbb{K}_2) = \boldsymbol{Q} * (\alpha \mathbb{K}_1) + \boldsymbol{Q} * \mathbb{K}_2, \tag{10}$$

it is possible to denote this with an 8^{th} order linear mapping $\overset{\langle 8 \rangle}{\mathbb{P}}$ as

$$\overline{\mathbb{K}}_{\mathcal{G}} = \overset{\langle 8 \rangle}{\mathbb{P}} :: \mathbb{K} \qquad \text{with} \tag{11}$$

$$\overset{\langle 8 \rangle}{\mathbb{P}} = \frac{1}{N} \sum_{z=1}^{N} Q^z_{im} Q^z_{jn} Q^z_{ko} Q^z_{lp} \boldsymbol{e}_i \otimes \boldsymbol{e}_j \otimes \boldsymbol{e}_k \otimes \boldsymbol{e}_l \otimes \boldsymbol{e}_m \otimes \boldsymbol{e}_n \otimes \boldsymbol{e}_o \otimes \boldsymbol{e}_p \tag{12}$$

which we label $\overset{\langle 8 \rangle}{\mathbb{P}}$ in anticipation of its projector properties. To demonstrate this property, we rotate the mean value with a second group element $\boldsymbol{Q}_y$.

$$\boldsymbol{Q}_y * \overline{\mathbb{K}}_{\mathcal{G}} = \frac{1}{N} \sum_{z=1}^{N} \boldsymbol{Q}_y * (\boldsymbol{Q}_z * \mathbb{K}) \tag{13}$$

$$= \frac{1}{N} \sum_{z=1}^{N} (\boldsymbol{Q}_y \boldsymbol{Q}_z) * \mathbb{K} \tag{14}$$

$$= \frac{1}{N} \sum_{z=1}^{N} \boldsymbol{Q}^*_z * \mathbb{K} \tag{15}$$

$$= \overline{\mathbb{K}}_{\mathcal{G}}. \tag{16}$$

The composition of $\boldsymbol{Q}_y$ and $\boldsymbol{Q}_z$ gives, following the group axioms, a mere re-indexing of the group members to $\boldsymbol{Q}^*_z$, which does not affect the result. $\overset{\langle 8 \rangle}{\mathbb{P}}$ acts as the identity on the set of all $\mathbb{K}$ which are $\mathcal{G}$-symmetric, and projects otherwise all non-$\mathcal{G}$-symmetric $\mathbb{K}$ into their $\mathcal{G}$-symmetric part.

The section is concluded by noting that the linearity of the Rayleigh product (eq. 10) in the second argument together with the definition of symmetry $\boldsymbol{Q}_i * \mathbb{K} = \mathbb{K}$ under the action of $\boldsymbol{Q}_i$ imply the convexity of the set of all tensors $\mathbb{K}$ that are invariant under the action of a certain symmetry group $\mathcal{G}$, i.e.

$$\text{If } \mathbb{K}_1, \mathbb{K}_2 \in \mathcal{K}_{\text{sym}} \text{ then } \alpha\mathbb{K}_1 + (1-\alpha)\mathbb{K}_2 \ \in \mathcal{K}_{\text{sym}} \ \forall\ \alpha \in [0,1]. \tag{17}$$

Because of the convexity of the subspace $\mathcal{K}_{\text{sym}} \subset \mathcal{K}$, the projection operation is unique. It is not hard to verify that the part of $\mathbb{K} - \overline{\mathbb{K}}_{\mathcal{G}}$ that is removed by the projection is perpendicular to the remainder $\overline{\mathbb{K}}_{\mathcal{G}}$, i.e.

$$(\mathbb{K} - \overline{\mathbb{K}}_{\mathcal{G}}) :: \overline{\mathbb{K}}_{\mathcal{G}} = 0. \tag{18}$$

This can be easily seen by expanding the right factor with the projector $\overline{\mathbb{K}}_{\mathcal{G}} = \overset{\langle 8 \rangle}{\mathbb{P}} :: \overline{\mathbb{K}}_{\mathcal{G}}$ and associating it with the left factor. In conjunction, the orthogonality and the uniqueness due to the convexity of the subset guarantee that the associated distance between $\mathbb{K}$ and $\overset{\langle 8 \rangle}{\mathbb{P}}\mathbb{K}$ is minimal. This has also been found by Gazis, Tadjbakhsh, and Toupin (1963), Sec. 2.

2.4 Minimization over the Euler angles

2.4.1 Rotation matrix

We have to minimize the distance between the arbitrarily oriented stiffness tetrad and a chosen fixed reference symmetry class. The orientation is parametrized by three Euler angles. We use the yaw-pitch-roll convention that rotates w.r.t. the fixed axes firstly by α around $\boldsymbol{e}_z$, then β around $\boldsymbol{e}_y$ and finally by γ around $\boldsymbol{e}_x$ (see Morawiec, 2004 Sec. 2.4.1). This leads to a component form of the rotation tensor

$$\boldsymbol{Q}_{\alpha,\beta,\gamma} = \begin{pmatrix} \cos\alpha\cos\beta & -\cos\beta\sin\alpha & \sin\beta \\ \cos\gamma\sin\alpha & \cos\alpha\cos\gamma & -\cos\beta\sin\gamma \\ +\cos\alpha\sin\beta\sin\gamma & -\sin\alpha\sin\beta\sin\gamma & \\ -\cos\alpha\cos\gamma\sin\beta & \cos\gamma\sin\alpha\sin\beta & \cos\beta\cos\gamma \\ +\sin\alpha\sin\gamma & +\cos\alpha\sin\gamma & \end{pmatrix} \boldsymbol{e}_i \otimes \boldsymbol{e}_j. \tag{19}$$

Again, the application of the Rayleigh product can be written as a linear mapping $\boldsymbol{Q}_{\alpha,\beta,\gamma} * \mathbb{K} = \overset{\langle 8 \rangle}{\mathbb{Q}}_{\alpha,\beta,\gamma} :: \mathbb{K}$ with an 8^{th} order tensor which covers the rotation

$$\overset{\langle 8 \rangle}{\mathbb{Q}}_{\alpha,\beta,\gamma} = Q_{im|\alpha,\beta,\gamma} Q_{jn|\alpha,\beta,\gamma} Q_{ko|\alpha,\beta,\gamma} Q_{lp|\alpha,\beta,\gamma} \boldsymbol{e}_i \otimes \boldsymbol{e}_j \otimes \boldsymbol{e}_k \otimes \boldsymbol{e}_l \otimes \boldsymbol{e}_m \otimes \boldsymbol{e}_n \otimes \boldsymbol{e}_o \otimes \boldsymbol{e}_p \tag{20}$$

2.5 Combination of projection and rotation

Finally we combine the 8^{th} order projection tensor $\overset{\langle 8 \rangle}{\mathbb{P}}$ and the 8^{th} order rotation tensor $\overset{\langle 8 \rangle}{\mathbb{Q}}_{\alpha,\beta,\gamma}$ to the final transformation

$$\overset{\langle 8 \rangle}{\mathbb{P}\mathbb{Q}}_{\alpha,\beta,\gamma} = \overset{\langle 8 \rangle}{\mathbb{P}} :: \overset{\langle 8 \rangle}{\mathbb{Q}}_{\alpha,\beta,\gamma} \,. \tag{21}$$

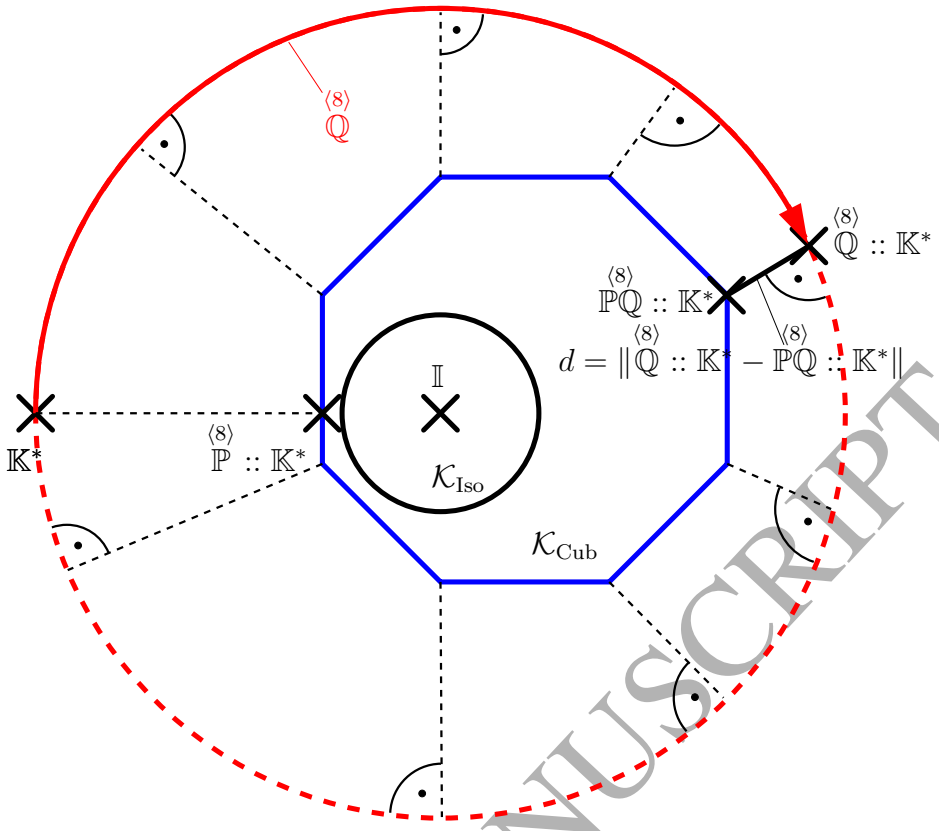

Figure 2: Schematic representation of the projection method. The paper plane represents all stiffness tetrads, where we pick some specific $\mathbb{K}^* = \mathbb{K}/\|\mathbb{K}\|$. The octagonal region is the subset of all cubic stiffness tetrads $\mathcal{K}_{\text{Cub}}$, w.r.t. fixed axes. Within this region the solid circle region represents the set of all isotropic stiffness tetrads $\mathcal{K}_{\text{Iso}}$ as a subset of the octagonal region. The outer circle section is a part of the orbit of $\mathbb{K}$ under the action of $\mathcal{O}rth^+$ depicted as the outer large dashed circle.

In the projection $\overset{\langle 8 \rangle}{\mathbb{PQ}}_{\alpha,\beta,\gamma}$ there are three unknown Euler angles α, β and γ. W.r.t. these angles, the Frobenius norm on fourth order tensors of the difference between the rotated $\mathbb{K}$ and the rotated and projected $\mathbb{K}$ has to be minimized. A sketch of the orbit and the projection to the symmetry groups is given in Figure 2. This procedure differs from Francois, Geymonat, and Berthaud (1998) since we first apply the rotation and then determine the relative distance to the symmetry classes.

$$d = \min_{i,\alpha,\beta,\gamma} \|\overset{\langle 8 \rangle}{\mathbb{Q}}_{\alpha,\beta,\gamma} :: \mathbb{K}^* - \overset{\langle 8 \rangle}{\mathbb{PQ}}_{\alpha,\beta,\gamma} :: \mathbb{K}^*\|, \qquad \mathbb{K}^* = \mathbb{K}/\|\mathbb{K}\|. \tag{22}$$

2.6 Distance to isotropy

In the case of isotropy, we have a continuous group with infinitely many members and generators. Therefore we have to apply a different method for defining distances with the isotropy class. For this purpose we use the isotropic projectors

$$\mathbb{K} = \lambda_1 \mathbb{P}_1 + \lambda_2 \mathbb{P}_2, \tag{23}$$

$$\mathbb{P}_1 = \frac{1}{3} \boldsymbol{I} \otimes \boldsymbol{I}, \tag{24}$$

$$\mathbb{P}_2 = \mathbb{I} - \mathbb{P}_1, \tag{25}$$

with $\mathbb{I}$ the identity tensor on symmetric second order tensors and the eigenvalues $\lambda_{1,2}$. The isotropic projectors map into isotropic 1- and 5-dimensional subspaces of the space of symmetric second order tensors, namely the spherical and deviatoric subspaces, respectively. Most important for our work is the fact that both of these subspaces are closed under all proper rotations $\boldsymbol{Q} \in \mathcal{O}rth^+$. Thus, from the discussion in the previous section we do not have to distinguish between a reference symmetry group and all isomorphic symmetry groups in the isotropic case. Consequently, the minimization over the three Euler angels is not needed and we can directly apply directly the derived 8^{th} order projector. Generalizing the sums from the discrete sets to integrals (Morawiec, 2004) we get

$$\mathbb{P}_{\text{iso}}^{\langle 8 \rangle} = \frac{1}{|\mathcal{O}rth^+|} \int_{\mathcal{O}rth^+} Q_{im} Q_{jn} Q_{ko} Q_{lp} \boldsymbol{e}_i \otimes \boldsymbol{e}_j \otimes \boldsymbol{e}_k \otimes \boldsymbol{e}_l \otimes \boldsymbol{e}_m \otimes \boldsymbol{e}_n \otimes \boldsymbol{e}_o \otimes \boldsymbol{e}_p \mathrm{d}\boldsymbol{Q} \tag{26}$$

$$= \mathbb{P}_1 \otimes \mathbb{P}_1 + \frac{1}{5} \mathbb{P}_2 \otimes \mathbb{P}_2. \tag{27}$$

2.7 Minimization procedure

The function value to be minimized is periodic due to the Euler angle parametrization. It is sufficient to consider the intervals $\alpha, \gamma \in [0, 2\pi)$ and $\beta \in [-\pi/2, \pi/2]$ for the three Euler angles. Especially when minimizing the distance of a highly symmetric stiffness tetrad to a high symmetric symmetry class (e.g. both cubic), the actual periodicity is much smaller than these intervals, and the global minimum has a large number of equivalent solutions in terms of the Euler angles. The most anisotropic case is when we seek the distance of a triclinic stiffness tetrad to the monoclinic symmetry class. In this situation, the global minimum which we seek is two-fold due to the one nontrivial symmetry operation in the monoclinic case (see Table 1 and Fig. 3). In all other cases the

multiplicity will be larger than two. It is therefore possible to halve the search interval without loss of information in general. However, the reduction of the search domain in the Euler angle space is not trivial, see Jöchen and Böhlke (2012). Nevertheless, in case of the monoclinic and the transversely isotropic distance functions, one can choose the symmetry group representation and the parametrization of $\mathcal{O}rth^+$ by the Euler angles α, β and γ such that the distance becomes independent of one of the Euler angles, see Diner, Kochetov, and Slawinski (2011). To reduce the numerical effort, we apply these simplifications, detailed in the supplementary material.

Further, it is a well known result from representation theory that at most a four-fold rotational symmetry can be distinguished in tetrads (Böhlke and Brüggemann, 2001). For example, hexagonal materials and quasi-crystals with a five-fold symmetry are not distinguishable from transversal isotropy in linear elasticity, but in case of higher order theories, like strain gradient elasticity (Olive and Auffray, 2013, 2014). Therefore, the frequencies at which the distance measure can oscillate over the Euler angles is at most $2\pi/4/4$, taking into account the potential fourfold symmetry of $\mathbb{K}$ and of the symmetry group. For our practical purpose, this means that a fixed discretization of a starting point grid is sufficient to guarantee the finding of the global minimum. This allows for an efficient and robust implementation. We employed a gradient based downhill search method from a conservative starting point grid of $8 \times 4 \times 8$ points in the space of Euler angles, with a spacing of $\pi/8$. It is clear that the discretization of rotations in terms of Euler angles is not optimal. The equidistant Euler angle grid results in cluster points in $\mathcal{O}rth^+$. To optimize the numerical effort, one may use starting points that correspond to a fair discretization of $\mathcal{O}rth^+$, see, e.g. Nawratil and Pottmann (2008). However, in our case, the additional effort is not justified, since we have a small grid of starting points and apply the distance minimization only to a few stiffness tetrads.

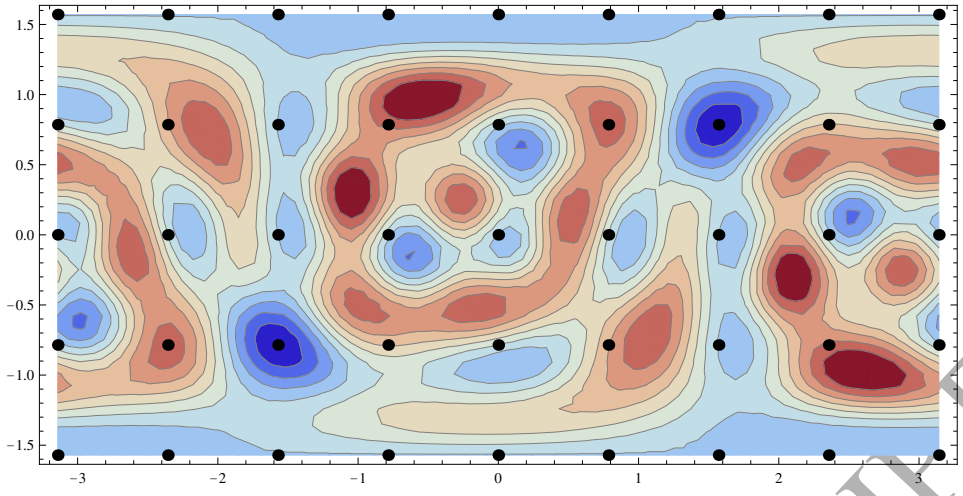

Figure 3: Minimization landscape when minimizing the distance d of a triclinic $\mathbb{K}$ to the monoclinic symmetry class, with γ fixed and d depending only on α (horizontal axes) and β (vertical axes). The local minima are colored in blue, local maxima are colored in red. One can see the poles ($\beta = \pm\pi/2$) and a grid (black points) of the initial values for the local minimization. The overall frequency of the extrema is $\pi/8$, but since they alternate, a spacing of $\pi/4$ is sufficient to detect all the local minima. One can see the presence of a two-fold global minimum.

3 Example applications

In the following subsections we apply the described method to determine the distance of the stiffness tetrads for an entirely artificial model material. We set up simulations of uni-, bi- and tridirectionally reinforced fiber-matrix materials, and examine the distances to the symmetry classes. To model the sample materials we use representative volume elements (RVE). This is done for two different deformation states. The first one is the initial state of the undeformed material sample. The second one is after a large deformation. We use isotropic elastoplastic material laws without hardening for both components. They are implemented in the user subroutine UMAT of the finite element program ABAQUS. The material parameters are Young's modulus E, Poisson's ratio ν and the v. Mises yield limit σ_{F}. The values for the matrix and fiber material are $E_{\mathrm{Matrix}} = 10\,000$ N/mm^2, $\nu_{\mathrm{Matrix}} = 0.3$, $\sigma_{\mathrm{F,Matrix}} = 100$ N/mm^2 for the matrix material, and $E_{\mathrm{Fiber}} = 100\,000$ N/mm^2, $\nu_{\mathrm{Fiber}} = 0.3$, $\sigma_{\mathrm{F,Fiber}} = 200$ N/mm^2 for the fibers. To determine the macroscopic stiffness tetrads we use the difference quotient out of six test calculations performing small elastic test strains in different directions. The stresses and the strains are measured in terms of the 2^{nd} Piola-Kirchhoff stress tensor $\overset{\mathrm{2PK}}{\boldsymbol{T}}$ and the Green strain tensor $\boldsymbol{E}^G$ in the reference placement. In the following we refer to the

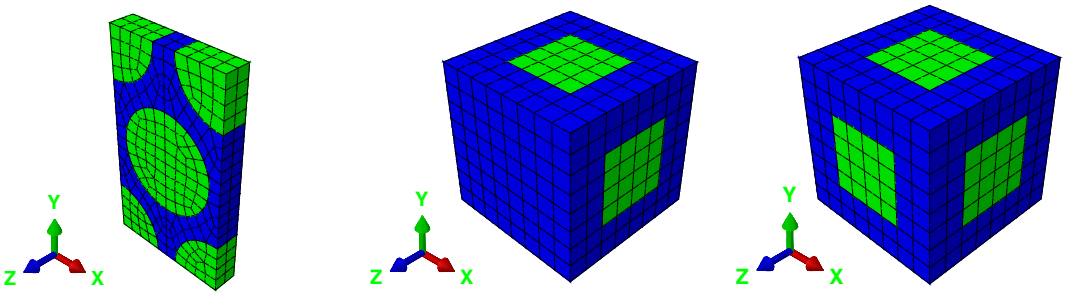

(a) unidirectional (b) bidirectional (c) tridirectional

Figure 4: Overview of the three sample materials

initial stiffness with $\mathbb{K}_0$ and to the stiffness of the plastically deformed material with $\mathbb{K}_1$. The first material is a unidirectionally reinforced composite with a hexagonal arrangement of the fibers. The effective elastic stiffness tetrad of this composite is transversely isotropic (see Figure 4(a)). The second sample material is a bidirectionally reinforced composite with a fiber angle of 90°. For this material the resulting effective elastic stiffness tetrad has a tetragonal symmetry (see Figure 4(b)). The third material is tridirectional reinforced material with a fiber angle of 90° between all the three fibers resulting in a cubic stiffness tetrad (see Figure 4(c)).

The three materials are modeled as representative volume elements (RVE) with periodic boundary conditions (see Glüge, Weber, and Bertram (2012)). The finite element simulation in ABAQUS is displacement controlled. We use the element type C3D20 which is a three dimensional element with a quadratic ansatz function (20 nodes). The stiffness tetrads are calculated in the reference placement. Since we have to compare them in their stress-free placement, we have to push forward $\mathbb{K}_1$ with the deformation gradient $\boldsymbol{F}$. The following figures show the distance d of the stiffness tetrad of the virgin (undeformed) material $\mathbb{K}_0$ (dark grey) and the stiffness tetrad of the deformed material after the different tests $\boldsymbol{F} * \mathbb{K}_1$ (light grey) to the symmetry classes. On the right hand side of each figure the shape of the undeformed and deformed material and its associated coordinate system are illustrated.

3.1 Results for the unidirectionally reinforced material

We know that the unidirectional reinforcement results in an hexagonal symmetry of the initial stiffness tetrad $\mathbb{K}_0$. We find this result in all the figures of this subsection ($d = 0\%$ for the dark grey bars of $\mathbb{K}_0$). The distance to all symmetry classes except the cubic and

the isotropic class is zero (see Figures 5 to 10).

3.1.1 Transverse fiber shift

In Figure 5 we see the situation after a shear test with $\gamma_{xy} = 0.5$. This deformation causes a movement of the fibers relative to each other. The fiber axis orientation remains unchanged. For the cubic symmetry class we find a distance of $d = 31\%$ and the distance to the isotropic symmetry class is $d = 33\%$. After the plastic deformation the stiffness tetrad has changed to $\mathbb{K}_1$. Following the results we find out that the symmetry of the deformed material is almost orthotropic. The reason is the shear number of $\gamma_{xy} = 0.5$ which leads to a closer fiber arrangement. The distance to the tetragonal symmetry is already $d = 5\%$ and to the initial hexagonal symmetry of the undeformed material d =8%. The same is true for a shear deformation with $\gamma_{yx} = 0.5$.

3.1.2 Fiber inclination

Figure 6 shows the results after the shear test with $\gamma_{xz} = 0.5$ (similar results are obtained using $\gamma_{yz} = 0.5$) which leads to the change of the fiber axes orientation. During the deformation the symmetry remains nearly the same, namely hexagonal. The negligible distances to the lower symmetry classes result from the fact that the inter-fiber distance is slightly decreased due to the fiber inclination.

3.1.3 Parallel fiber shift

In Figure 7 we find no change regarding the symmetry since the shear $\gamma_{zx} = 0.5$ test alone caused only a parallel shift of the fibers. There is no shift of the fibers and no change of the axes. This is again true for the shear deformation $\gamma_{zy} = 0.5$.

3.1.4 Elongation tests

In case of a tension test with $\epsilon_{xx} = 0.5$ as depicted in Figure 8 the material symmetry becomes tetragonal with a distance of less than 5%. For the trigonal and the initial hexagonal class the distance results in about 5%. The same is true for a tension test with $\epsilon_{yy} = 0.5$ because the hexagonal fiber arrangement is destroyed during this deformations. For a tension test in fiber direction (see Figure 9), $\epsilon_{zz} = 0.5$, there is no change of the material symmetry because the fibers are only elongated along their axes.

3.1.5 Mixed mode test

The results for the last test calculation (Figure 10) with a shear deformation of $\gamma_{xy} = \gamma_{xz} = 0.5$ and a uniaxial tension of $\epsilon_{xx} = 0.5$ (applied simultaneously) shows a similar behavior of the symmetry change compared to the first test case with $\gamma_{xy} = 0.5$ because the shear in this direction leads to the largest symmetry change. After the deformation there is a distance of around 5% to the trigonal and the hexagonal symmetry. But we find that the material can be considered as tetragonal with a distance of only 2%.
In summary it turns out that the plastic deformation of the uniaxial deformed material leads to a change of the symmetry of the stiffness tetrad. The initial stiffness tetrad has the hexagonal symmetry. In all cases the symmetry of the stiffness tetrad $\mathbb{K}_1$ after the deformation is at least orthotropic. The distance to the tetragonal, trigonal and hexagonal symmetry classes remains in the range between 0% and 8%.

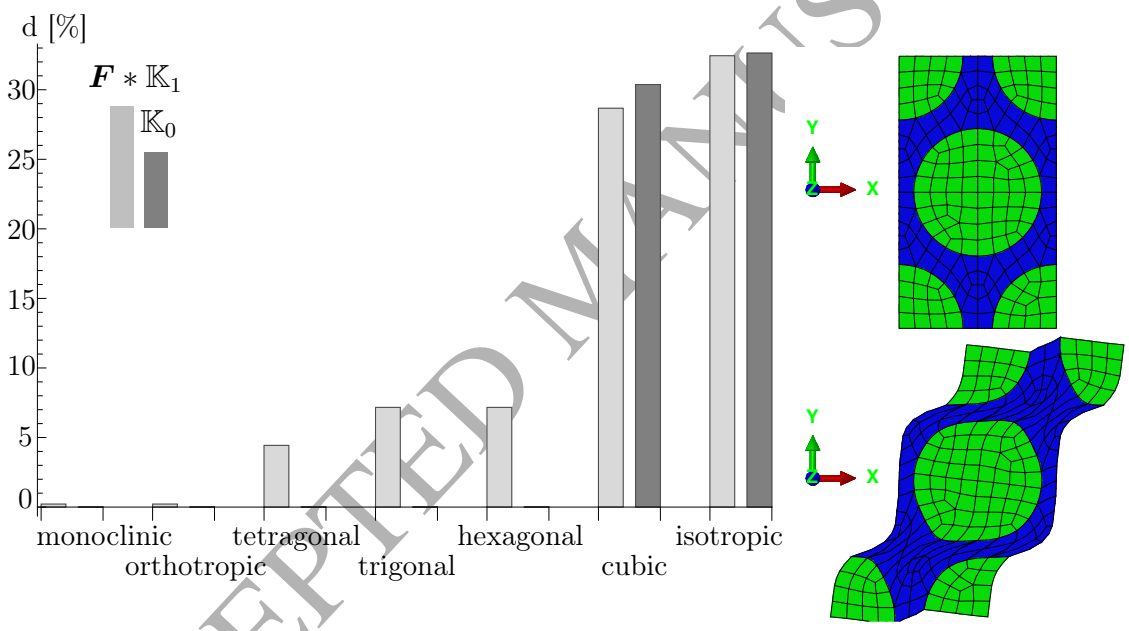

Figure 5: Distance d to the symmetry classes after the deformation $\gamma_{xy} = 0.5$

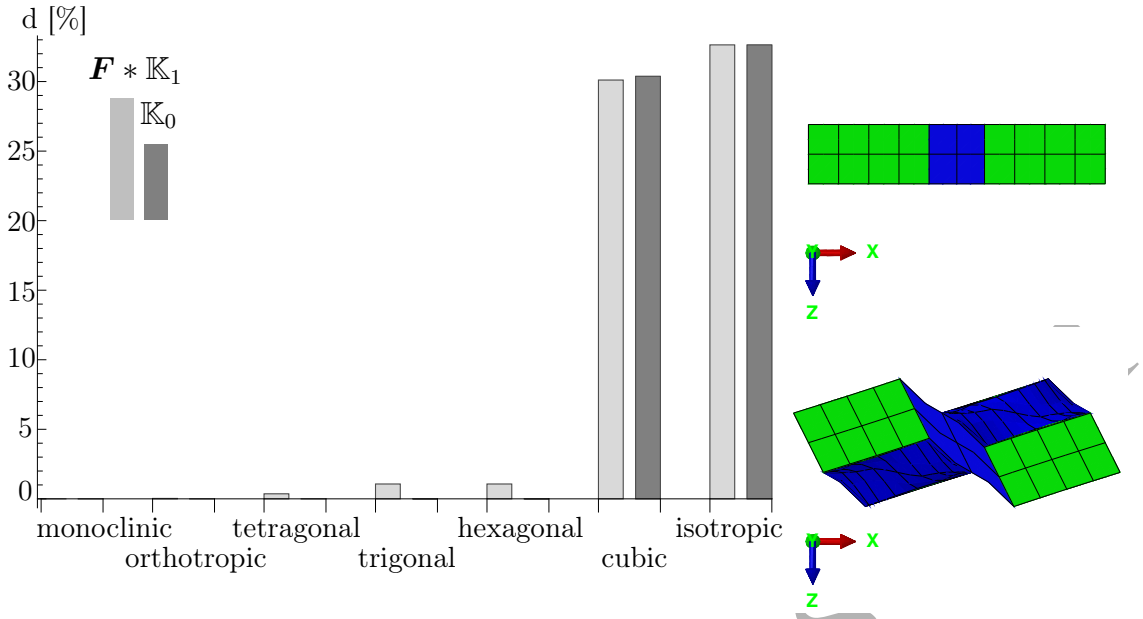

Figure 6: Distance d to the symmetry classes after the deformation $\gamma_{xz} = 0.5$

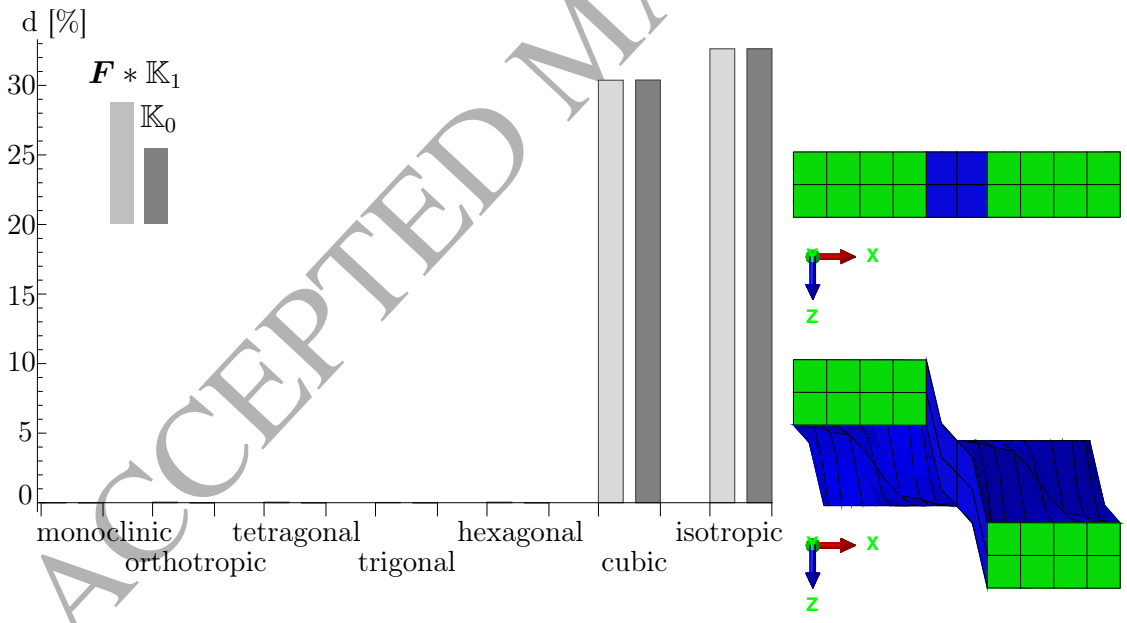

Figure 7: Distance d to the symmetry classes after the deformation $\gamma_{zx} = 0.5$

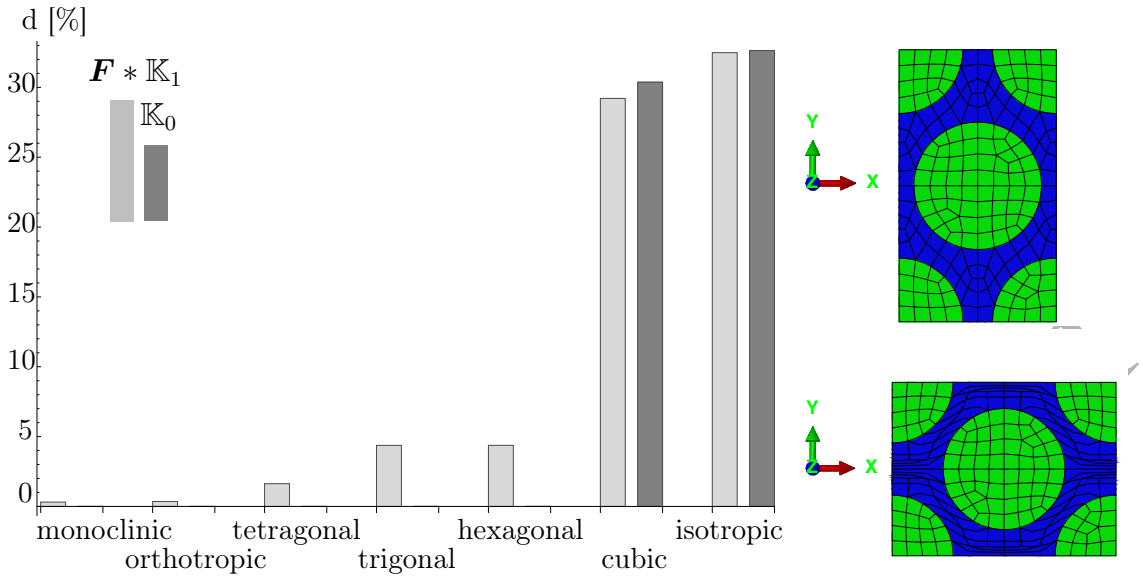

Figure 8: Distance d to the symmetry classes after the deformation $\epsilon_{xx} = 0.5$

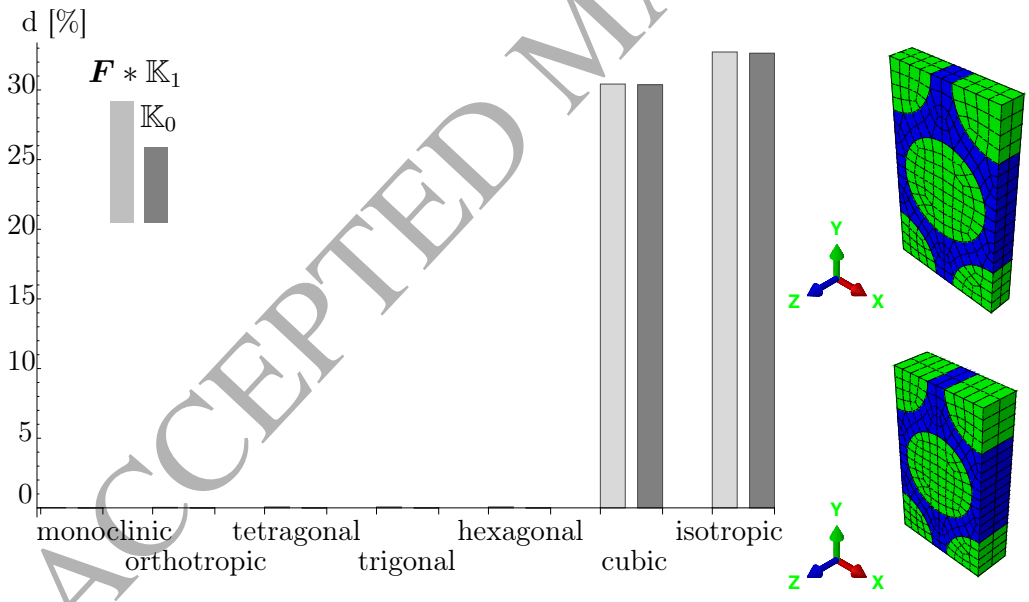

Figure 9: Distance d to the symmetry classes after the deformation $\epsilon_{zz} = 0.5$

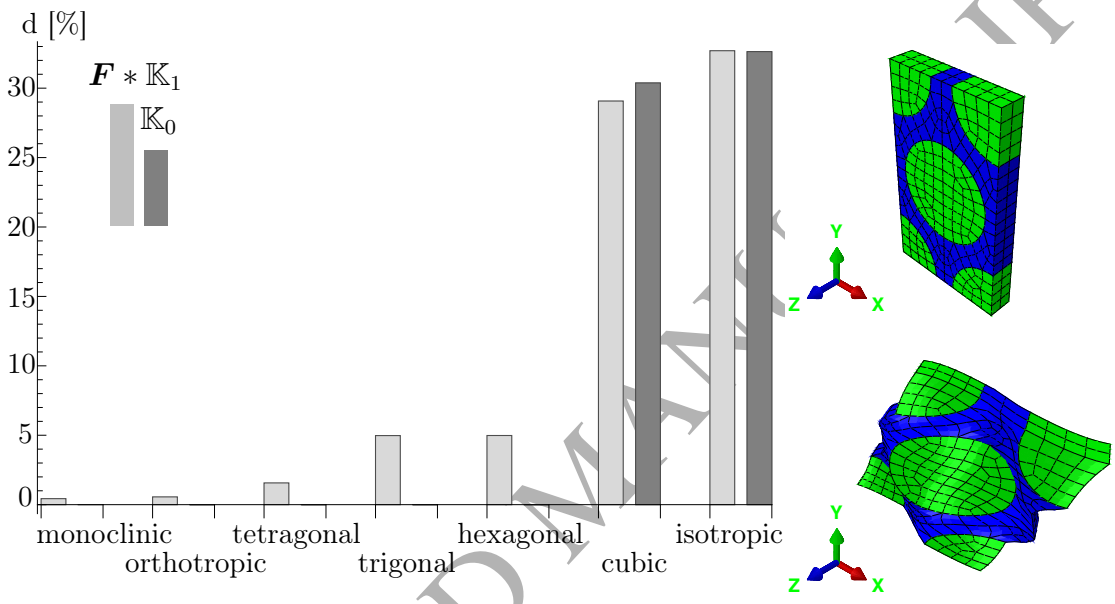

Figure 10: Distance d to the symmetry classes after the deformation $\gamma_{xy} = \gamma_{xz} = 0.5$ and $\epsilon_{xx} = 0.5$

3.2 Results for the bidirectionally reinforced material

The undeformed bidirectionally reinforced material $\mathbb{K}_0$ has the tetragonal symmetry (see Figure 11).

3.2.1 Shear in the fiber plane

After the shear test $\gamma_{xy} = 0.5$ the material can be considered as orthotropic because the distance d for $\mathbb{K}_1$ is 15,5% to the tetragonal symmetry but less than 1% to the orthotropic symmetry class. Similar results are obtained by the shear deformation $\gamma_{yx} = 0.5$. The reason for the large distance to the initial tetragonal symmetry is the change of the angle between the fibers during the deformation.

3.2.2 Shear parallel to the fibers

In Figure 12 we find that the material nearly remains tetragonal with a distance of less than 3% after the deformation $\gamma_{xz} = 0.5$ (also true for the deformation $\gamma_{yz} = 0.5$). This is because the angle between the fibers does not change during this shear deformation in contrast to the in-plane shear.

3.2.3 Fiber plane inclination

For the deformations $\gamma_{zx} = 0.5$ (see Figure 13) or $\gamma_{zy} = 0.5$ the distance to the initial tetragonal symmetry class also remains in the range of less than 3% which again results from the unchanged angle between the fibers. The results differ slightly from the foregoing case since the planes spanned by the fibers come closer together in the present case. Also, one fiber gets stretched, while the other is only displaced transversally.

3.2.4 Elongation tests

In Figure 14 the material symmetry has to be considered as trigonal after the elongation $\epsilon_{xx} = 0.5$ because the distance to the tetragonal class is nearly 5%. The reason is that after the deformation the spacing between the fibers in y direction is larger than the spacing between the fibers in x direction. The same is true for an elongation test in y direction.

Only in the case of an elongation test in z direction as depicted in Figure 15 the material symmetry remains unchanged after the deformation because the fiber spacing changes simultaneously and remains the same in both x and y directions.

3.2.5 Mixed mode test

The deformation with shear $\gamma_{xy} = \gamma_{xz} = 0.5$ and uniaxial tension $\epsilon_{xx} = 0.5$ (applied simultaneously) as shown in Figure 16 results in an orthotropic material. The distance to the tetragonal symmetry class is about 15%.

Summarizing, the initial elastic behavior of the bidirectionally reinforced material is tetragonal. After different deformations the material remains at least orthotropic.

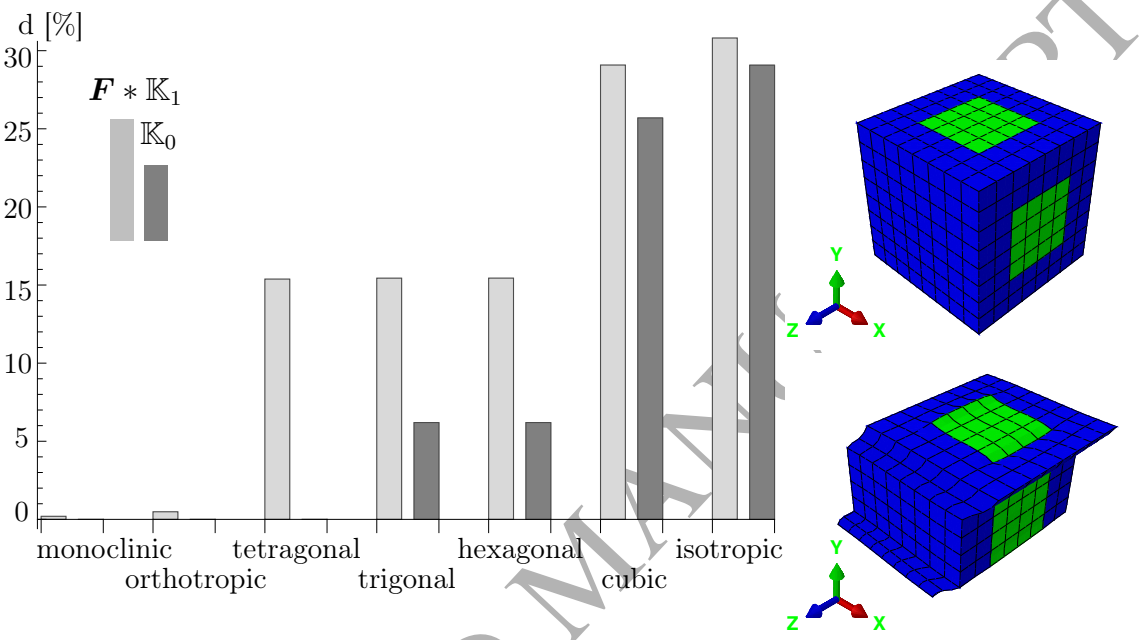

Figure 11: Distance d to the symmetry classes after the deformation $\gamma_{xy} = 0.5$

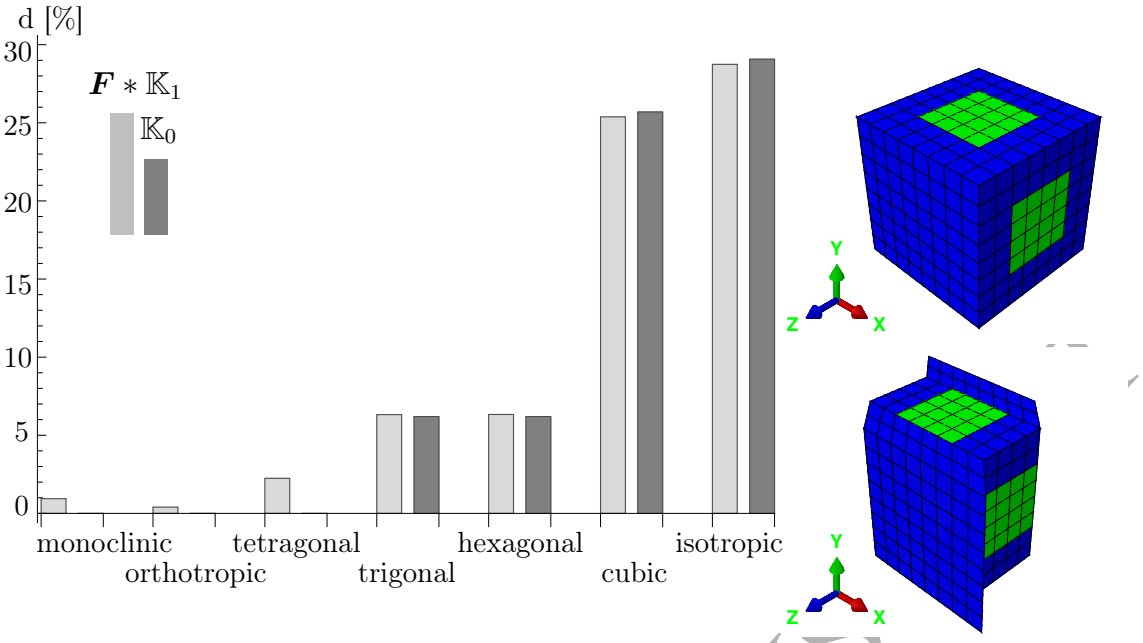

Figure 12: Distance d to the symmetry classes after the deformation $\gamma_{xz} = 0.5$

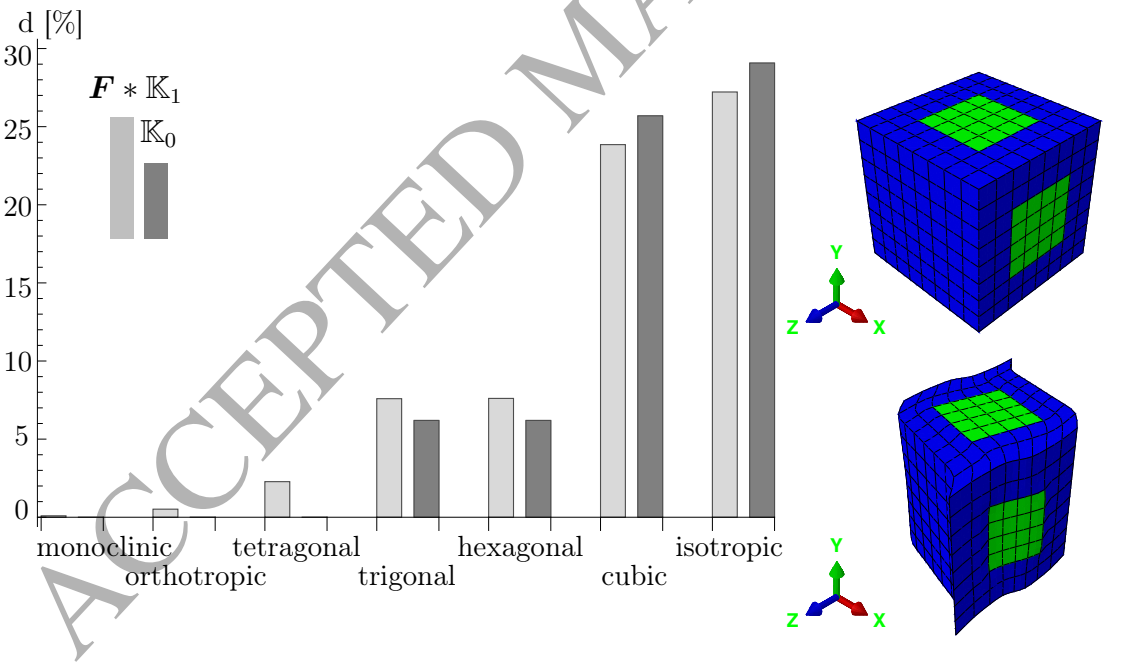

Figure 13: Distance d to the symmetry classes after the deformation $\gamma_{zx} = 0.5$

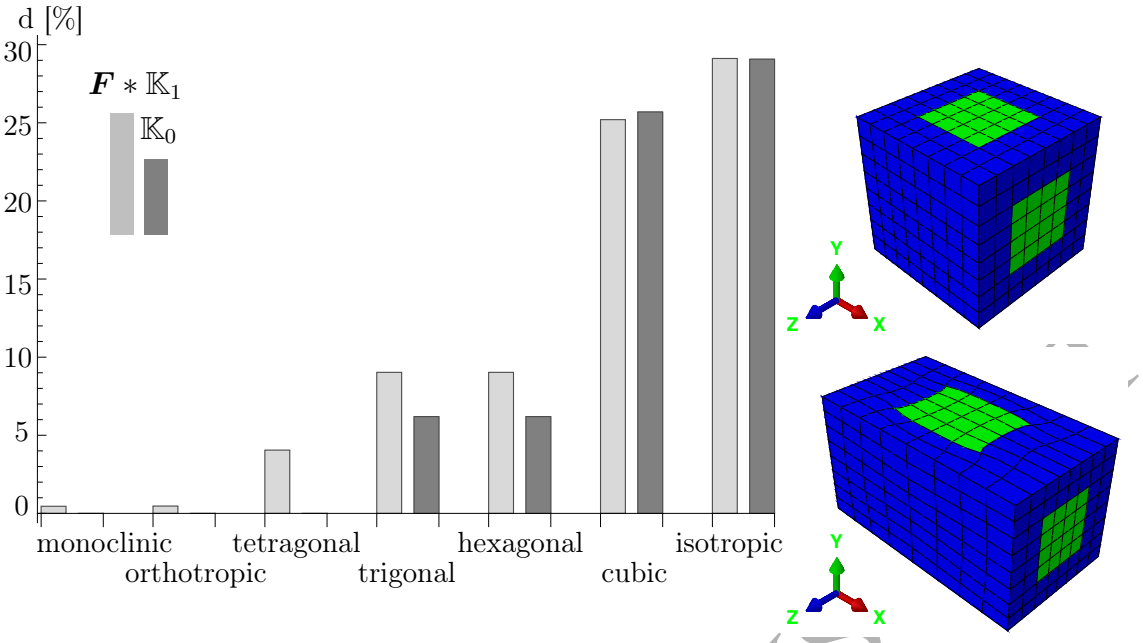

Figure 14: Distance d to the symmetry classes after the deformation $\gamma_{xx} = 0.5$

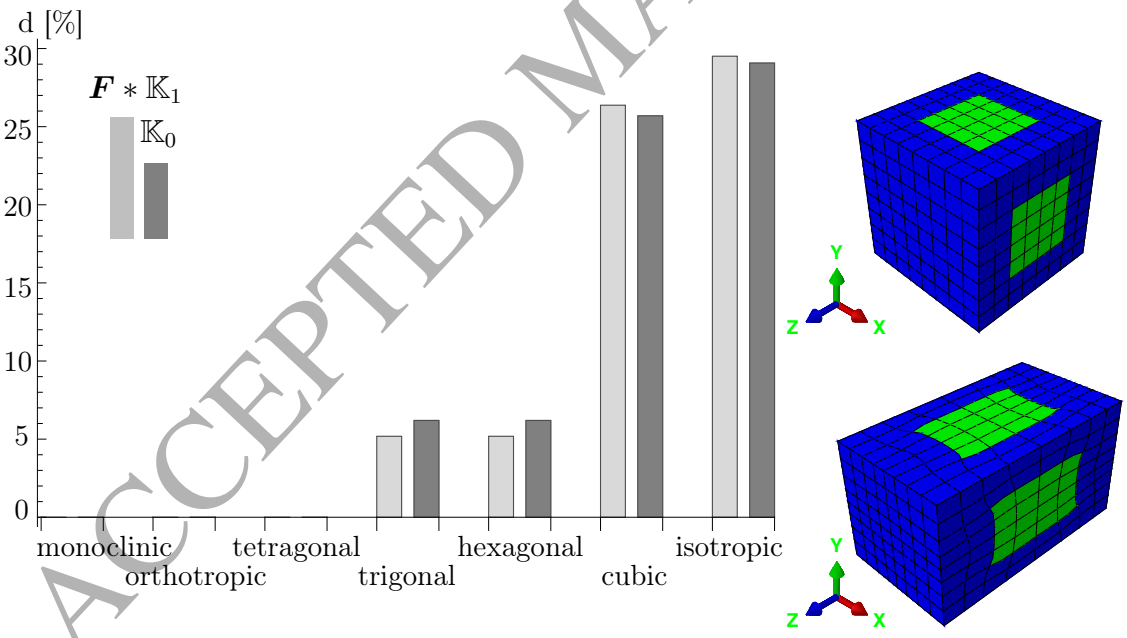

Figure 15: Distance d to the symmetry classes after the deformation $\gamma_{zz} = 0.5$

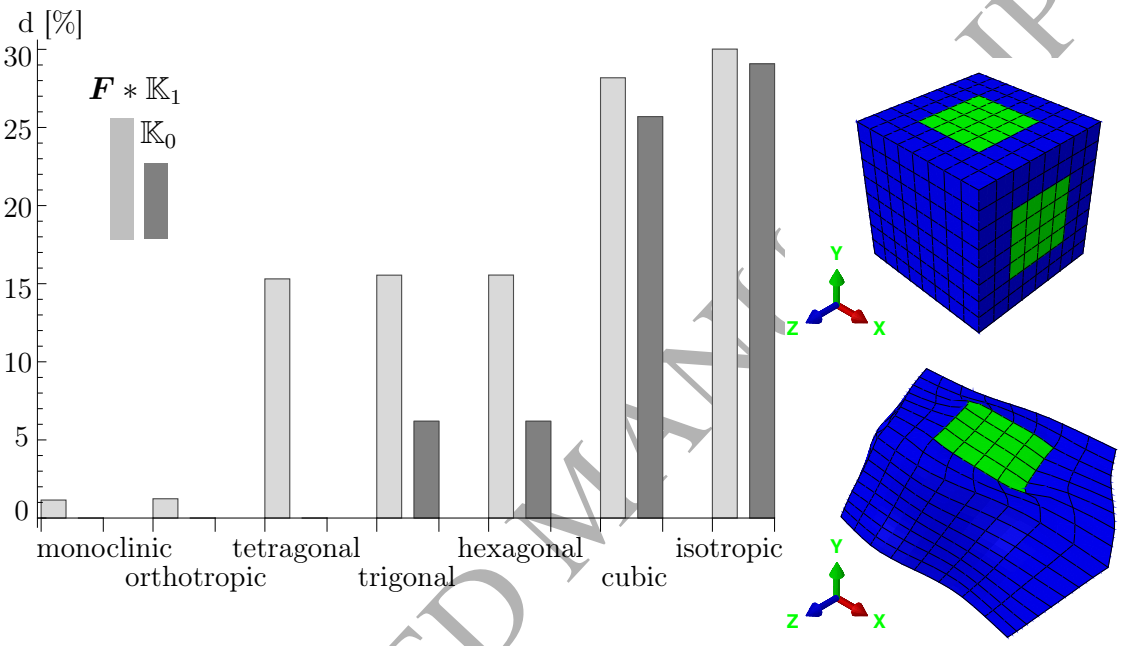

Figure 16: Distance d to the symmetry classes after the deformation $\gamma_{xy} = \gamma_{xz} = 0.5$ and $\epsilon_{xx} = 0.5$

3.3 Results for the tridirectionally reinforced material

The initial stiffness tetrad $\mathbb{K}_0$ of the tridirectionally reinforced material has a cubic symmetry. We find a distance of about 7% to the hexagonal and about 12% to the isotropic symmetry class for the dark grey bars of $\mathbb{K}_0$ in the following three figures (17 to 19). The trigonal symmetry is included, as the three-fold rotation around the cube's space diagonal is a symmetry operation.

3.3.1 Shear tests

Figure 17 shows that after a shear test $\gamma_{xy} = 0.5$ (true for all other shear tests with shear direction and shear plane normal parallel to the fiber axes) the material becomes orthotropic with a distance of only 1% to this class. To all other higher symmetry classes including the initial cubic one the distances are around 10%.

3.3.2 Elongation tests

By elongating the material parallel to a fiber (example depicted in Figure 18) with $\epsilon_{xx} = 0.5$ the distance to the cubic symmetry class increases but remains below 5%. The same is true for the trigonal and tetragonal symmetry classes. The reason is that the fiber spacing is not the same in all three directions after the deformation.

3.3.3 Mixed mode test

The deformation with shear $\gamma_{xy} = \gamma_{xz} = 0.5$ and uniaxial tension $\epsilon_{xx} = 0.5$ (applied simultaneously) in Figure 19 results in a triclinic material because the distance to all material symmetry classes is clearly larger than 5%.

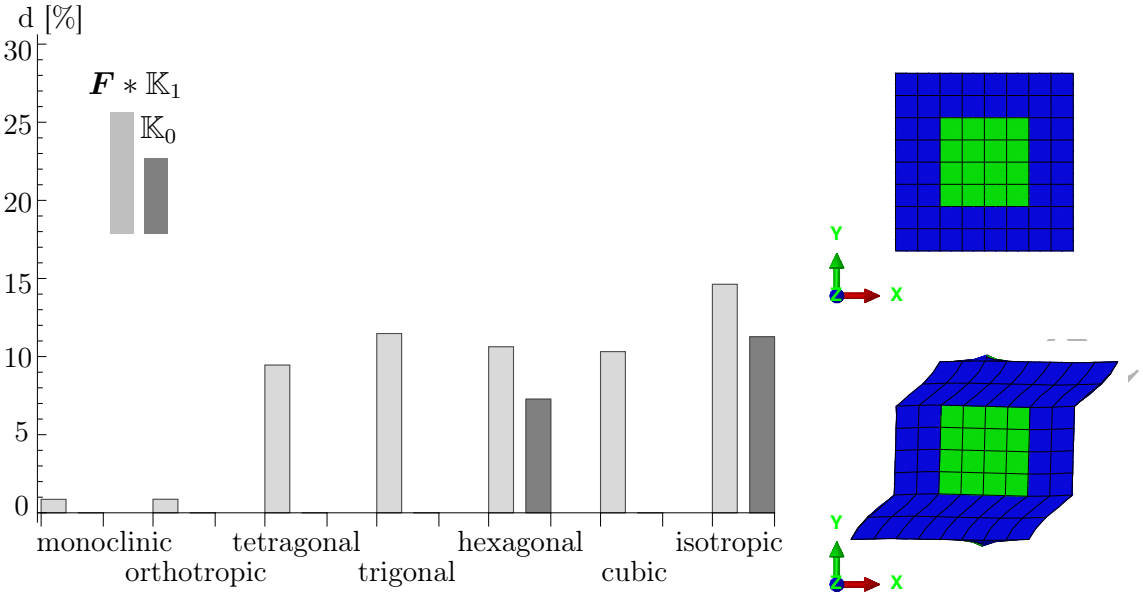

Figure 17: Distance d to the symmetry classes after the deformation $\gamma_{xy} = 0.5$

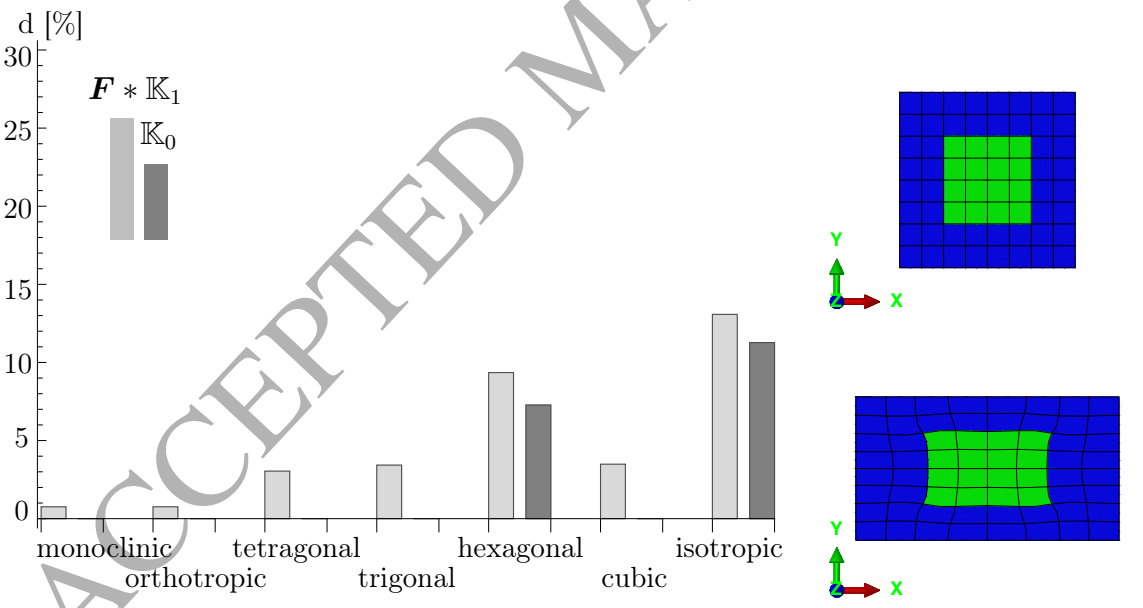

Figure 18: Distance d to the symmetry classes after the deformation $\epsilon_{xx} = 0.5$

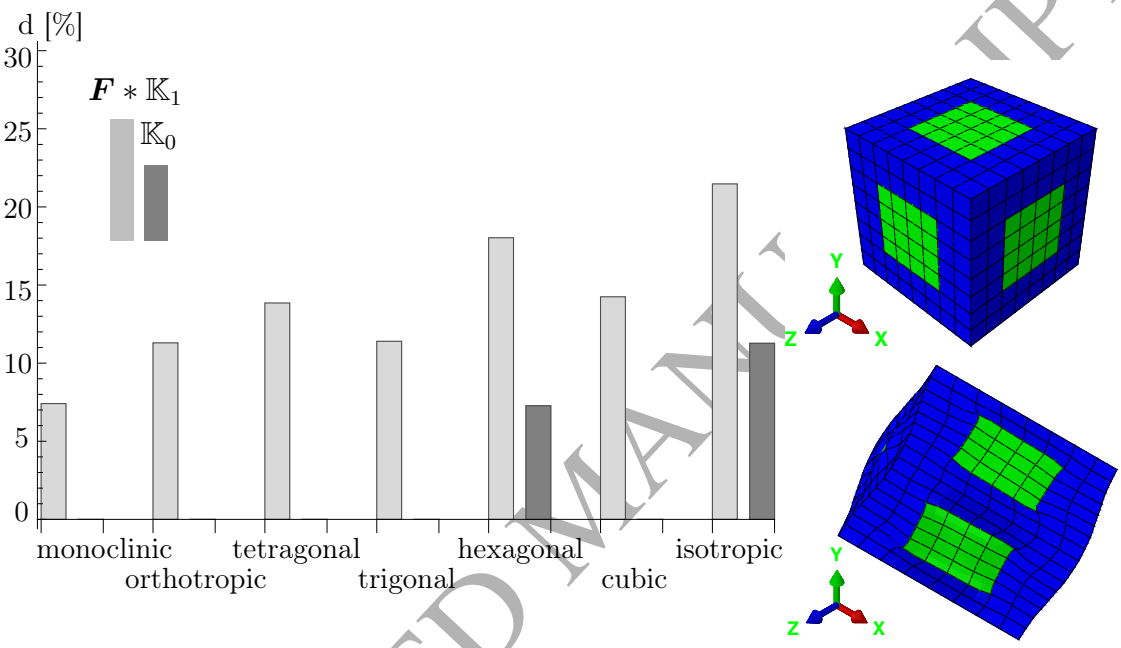

Figure 19: Distance d to the symmetry classes after the deformation $\gamma_{xy} = \gamma_{xz} = 0.5$ and $\epsilon_{xx} = 0.5$

4 Summary

In this paper we presented a fast algorithm to determine the distance of a measured stiffness tetrad to all tetrads with a certain symmetry. Using a projection method we build up an 8^{th} order tensor containing all group elements of the chosen group. After applying this projector to a given stiffness tetrad, we only have to minimize over the orientation of the symmetry axis and therefore only over the three Euler angles. Using this method we investigated a uni-, bi- and tridirectionally reinforced material submitted to large deformations.

In all cases, the distance measures corresponded well to the apparent symmetry classes. For example, all bidirectionally reinforced materials (Sec. 3.2) are very close to the orthotropic symmetry class. The deviations are due to inhomogeneous deformations inside the RVE, while the general proximity to the orthotropic symmetry class is due to the fact that in any bidirectional material with equal fiber properties, three orthogonal directions can be found, namely the fiber plane normal and the two angle bisectors. Other tests of plausibility, like the presence of trigonal symmetry around the 111-direction in an orthogonal tridirectional fiber arrangement in the (100) directions are captured as well (Sec. 3.3).

The proposed methodology relies on the robust determination of the global minimum of the distance measure over the orientation in terms of Euler angles. Since there are local minima, a simple gradient approach starting from one point is not sufficient, and precautions must be taken to ensure the finding of the global minimum. However, this is not difficult. As the Euler angle space is periodic and may be further reduced by invoking symmetries from the classes to which the stiffness is projected, it is sufficient to consider a small minimization domain. We never observed results that are contradictory to the symmetry class inclusion scheme, see Figure 1 (i.e. the distance to the tetragonal class is always smaller or equal to the distance to the cubic class, which renders the presented scheme applicable in an algorithmic manner) which makes us confident that the applied method is reliable.

5 Bibliography

Butler, P.H. (1981). *Point group symmetry applications: methods and tables*. Plenum Press. ISBN: 9780306405235 (cit. on p. 2).

Bóna, A., I. Bucataru, and A. Slawinski (2004). "Material Symmetries of Elasticity Tensors". In: *The Quarterly Journal of Mechanics and Applied Mathematics* 54.4, pp. 584–598. DOI: 10.1007/s10659-004-7192-0 (cit. on p. 6).

Böhlke, T. (2001). "Crystallographic Texture Evolution and Elastic Anisotropy: Simulation, Modeling and Applications". PhD thesis. Otto-von-Guericke University Magdeburg (cit. on p. 3).

Böhlke, T. and C. Brüggemann (2001). "Graphical Representation of the Generalized Hooke's Law". In: *Technische Mechanik* 21, pp. 145–158 (cit. on p. 13).

Cowin, S. C. and M. M. Mehrabadi (1987). "On the identification of material symmetry for anisotropic elastic materials". In: *The Quarterly Journal of Mechanics and Applied Mathematics* 40.4, pp. 451–476. DOI: 10.1093/qjmam/40.4.451 (cit. on p. 4).

Curie, P. (1894). "Sur la symétrie dans les phénomènes physiques, symétrie d'un champ électrique et d'un champ magnétique". In: *Journal de Physique* 3, pp. 393–415 (cit. on p. 2).

Diner, Ç., M. Kochetov, and M.A. Slawinski (2011). "Identifying Symmetry Classes of Elasticity Tensors Using Monoclinic Distance Function". In: *Journal of Elasticity* 102.2, pp. 175–190 (cit. on pp. 3, 13).

Fedorov, F.I. (1968). *Theory of elastic waves in crystals*. Plenum Press (cit. on p. 3).

Forte, S. and M. Vianello (1996). "Symmetry classes for elasticity tensors". In: *Journal of Elasticity* 43.2, pp. 81–108 (cit. on p. 2).

Francois, M., G. Geymonat, and Y. Berthaud (1998). "Determination of the symmetries of an experimentally determined stiffness tensor; application to acoustic measurements". In: *International Journal of Solids and Structures* 35.31-32, pp. 4091–4106 (cit. on pp. 3, 4, 11).

Gazis, D.C., I. Tadjbakhsh, and R.A. Toupin (1963). "The elastic tensor of given symmetry nearest to an anisotropic elastic tensor". In: *Acta Crystallographica* 16.9, pp. 917–922 (cit. on pp. 3, 10).

Glüge, R., M. Weber, and A. Bertram (2012). "Comparison of spherical and cubical statistical volume elements with respect to convergence, anisotropy, and localization behavior". In: *Computational. Material Science* 63, pp. 91–104. DOI: doi.org/10.1016/j.commatsci.2012.05.063 (cit. on pp. 3, 15).

Guilleminot, J. and C. Soize (2010). "A stochastic model for elasticity tensors with uncertain material symmetries". In: *International Journal of Solids and Structures* 47.22-23, pp. 3121–3130. DOI: 10.1016/j.ijsolstr.2010.07.013 (cit. on pp. 2, 3).

Jöchen, K. and T. Böhlke (Apr. 2012). "Prediction of Texture Evolution in Rolled Sheet Metals by Using Homogenization Schemes". In: *Material Forming ESAFORM 2012*. Vol. 504. Key Engineering Materials. Trans Tech Publications, pp. 649–654. DOI: 10.4028/www.scientific.net/KEM.504-506.649 (cit. on p. 13).

Kochetov, M. and M.A. Slawinski (2009). "On Obtaining Effective Transversely Isotropic Elasticity Tensors". In: *Journal of Elasticity* 94.1, pp. 1–13 (cit. on p. 3).

Moakher, M. and A. N. Norris (2006). "The Closest Elastic Tensor of Arbitrary Symmetry to an Elasticity Tensor of Lower Symmetry". In: *Journal of Elasticity* 85.3, pp. 215–263. DOI: 10.1007/s10659-006-9082-0 (cit. on p. 3).

Morawiec, A. (2004). *Orientations and Rotations– Computations in Crystallographic Textures*. Springer (cit. on pp. 10, 12).

Nawratil, G. and H. Pottmann (2008). "Subdivision schemes for the fair discretization of the spherical motion group". In: *Journal of Computational and Applied Mathematics* 222.2, pp. 574–591 (cit. on p. 13).

Neumann, F.E. (1885). *Vorlesungen über die Theorie der Elastizität der festen Körper und des Lichtäthers*. Ed. by O.E. Meyer. Teubner-Verlag Leipzig (cit. on p. 2).

Norris, A.N. (2006). "Elastic moduli approximation of higher symmetry for the acoustical properties of an anisotropic material". In: *Journal of the Acoustical Society of America* 119.4, pp. 2114–2121. DOI: 10.1121/1.2173525 (cit. on p. 2).

Olive, M. and N. Auffray (2013). "Symmetry classes for even-order tensors". In: *Mathematics and Mechancis of Complex Systems* 1.2, pp. 177–210. DOI: dx.doi.org/10.2140/memocs.2013.1.177 (cit. on p. 13).

Olive, M. and N. Auffray (2014). "Symmetry classes for odd-order tensors". In: *Zeitschrift für Angewandte Mathematik und Mechanik* 94.5, pp. 421–447. DOI: 10.1002/zamm.201200225 (cit. on pp. 2, 13).

Zou, W.N., C.X. Tang, and W.H. Lee (2013). "Identification of symmetry type of linear elastic stiffness tensor in an arbitrarily orientated coordinate system". In: *International*

Journal of Solids and Structures 50.14-15, pp. 2457–2467. DOI: doi.org/10.1016/j.ijsolstr.2013.03.037 (cit. on pp. 3, 4).